Journal of the European Ceramic Society 17 (1997) 831–841

PII: S0955-2219(96)00186-0
0955-2219/97/$17.00

Production of Defect-Poor Nanostructured Ceramics of Yttria–Zirconia

C. D. Sagel-Ransijn, A. J. A. Winnubst, B. Kerkwijk, A. J. Burggraaf & H. Verweij

University of Twente, Faculty of Chemical Technology, Laboratory for Inorganic Materials Science, Enschede, The Netherlands

(Received 23 July 1996; accepted 29 August 1996)

Abstract

For the production of nanostructured ceramics of yttria–zirconia four powders differing in agglomerate strength, agglomerate size and crystallite size are compared. An ultra-fine-grained ceramic with a final density of 98% and a grain size of 0·18 μm could be produced from a hydrothermally crystallized ethanol-washed powder. The remaining porosity is caused by some residual defects which are present due to the irregular shape of the agglomerates and which cause improper die filling. A commercially available powder was also investigated. This powder consists of homogeneous porous, spherical, weak agglomerates. The resulting ceramic has a high density (≥ 99%) but cannot be obtained with ultra-fine grain size (minimum grain size is 0·3 μm). The air-crystallized ethanol-washed powder resulted, after sintering, in larger porosities. In this case the powder consists of weak and some strong agglomerates and a few defect clusters are found in the sintered ceramic which limit the maximum attainable density to 92%. The air-crystallized water-washed powder consists of agglomerates which are too strong to be fractured during compaction. The sintered ceramics contain a large amount of porosity (20%) which is attributed to the presence of inter-agglomerate pores. © *1997 Elsevier Science Limited. All rights reserved.*

1 Introduction

High wear resistance and good mechanical properties of ceramic materials are required in order to have a wide range of structural applications. He *et al.*[1,2] showed that fine-grained zirconia exhibits better wear resistance compared to coarse-grained materials. For a similar material Theunissen *et al.*[3,4] found that both bending strength and fracture toughness at high temperatures are improved when the ceramic grain size decreases. Furthermore, by reducing the grain size to the nanocrystalline range, the superplastic deformation rates can be enhanced which can lead to industrial forming operations.[5,6] Thus, interesting structural properties can be expected for nanostructured zirconia (grain size < 100 nm).

The strength of ceramic materials is sensitive to the presence of flaws and their size. If the flaw size can be reduced or if flaws in the ceramic can be prevented or removed, strength will increase. For that reason zirconia should not only be nanostructured, but also defect-poor. In order to obtain dense, defect-poor, nanostructured yttria-doped tetragonal zirconia ceramics, special requirements must be fulfilled by the powders used for the sintering process. The powders should have a well-defined geometrical shape and be highly sinteractive (low sintering temperature) in order to restrict grain growth and defect formation during sintering. Homogeneous, nanocrystalline powders can be achieved by means of wet chemical methods such as sol–gel or gel–precipitation. Mono-disperse fine-grained (nanosized) powders are very difficult to produce but generally consist of larger, clustered microstructural elements.[7–11] The composing elements are primary crystallites, aggregates where the primary crystallites are held together by necks[7] and agglomerates with relatively weak (e.g. van der Waals, capillary) attractive forces.

In powder compacts three types of pore radii might be found: (1) intra-aggregate pores (pores between the primary crystallites within an aggregate); (2) inter-aggregate or intra-agglomerate pores (hereafter called first generation pores); (3) inter-agglomerate pores (hereafter called second generation pores). Thus the pore structure of compacts generally has an hierarchical character. A schematic representation of such a structure is given in Fig. 1. During sintering all pores must be eliminated from the compact to obtain dense, defect-poor ceramics.

Fig. 1. Scheme of particle packing in compacts prepared from agglomerated powders.

A common route for powder consolidation involves cold-pressing of dry powders. During compaction a nonuniform density distribution very often arises in the green compact. Density variations in the green compact may cause flaws in the sintered material. This non-uniformity can already be established during die-filling. Powder particles that are heaped up or otherwise nonuniformly stacked in the die may not reposition during pressing. A second source of density variation is friction between the powder and the die wall and between the powder particles. A third source of nonuniform green density is the presence of strong agglomerates in the powder or a range of agglomerate strengths. The strong agglomerates will shield weaker powder or agglomerates from exposure to the maximum applied pressure, resulting in flaw clusters that reduce strength. Although the applied pressure may break up many of the weak agglomerates and some of the strong agglomerates, experiments show that both types can persist after the pressing consolidation step.[12] Finally, the presence of both dense[13] and porous[12] agglomerates in a relatively weak matrix leads to the appearance of internal crack-like voids during sintering.

In this paper the influence of powder synthesis and powder processing on the change in first- and second-generation pore characteristics during consolidation and sintering of nanocrystalline powders is studied. Three ultra-fine powders have been used. A commercially available spray-dried, free-flowing powder (Tosoh TZ-3Y) was used for comparison.

2 Experimental Procedure

2.1 Powder synthesis

Appropriate amounts of $ZrCl_4$ (>98% pure) and YCl_3 (99·9% pure) for the preparation of Tetragonal Zirconia Polycrystals (TZP) with 5 at% Y on the Zr-site were dissolved in a 0·2 M aqueous HCl solution. The solution was filtered and added drop-wise to an excess of a 25 wt% ammonia solution, with the pH maintained at a value >11. A precipitated gel was obtained that was allowed to settle overnight, after which the clear supernatant was removed. The gel obtained was washed with water/ammonia mixtures until the washing liquid did not become turbid on addition of 0·1 M $AgNO_3$, an indication that the washing liquid is chloride-free. The gel was subsequently filtered. Part of the gel was redispersed in ethanol and subsequently washed three times in ethanol. The ethanol- and water-washed gels were both dried at 120°C. Crystallization of the gels took place in static air or under hydrothermal conditions.

The water-washed and part of the ethanol-washed gel were dry-milled and calcined in static air at 500°C for 2 h. After heat-treatment the calcined water-washed gel was dry-milled again, whereas the calcined ethanol-washed gel was wet-milled in ethanol using nylon balls in a polyethylene container. Wet-milling took place in a wrist-action shaker (Turbula T2C). After wet-milling, the suspension was sieved through a sieve with 38 μm mesh size in order to remove remaining large agglomerates and contamination. After drying the suspension at 120°C, the powder was sieved through a 180 μm mesh sieve. The calcined and only water-washed gel is coded as AC-WW, whereas the calcined ethanol-washed gel is coded AC. (Explanation of codes is given in Table 1.)

The other part of the ethanol-washed gel was used for hydrothermal crystallization in a stainless-steel autoclave equipped with a PTFE liner. Crystallization of the gel took place at 200°C for 2 h in a basic medium (ammonia solution) at a pressure of 20–30 bar. After hydrothermal treatment the pH of the slurry was 9–11. The slurry was transferred into a polyethylene vessel together with zirconia balls and a large amount of ethanol and put on a roller bench for 1 h. The slurry was allowed to settle overnight, after which the clear supernatant was removed. This washing step was repeated three times after which the slurry was filtered and dried at 120°C. This powder was dry-milled and heat-treated at 400°C for 1 h to remove residual organics. After heat-treatment the powder was wet-milled and sieved as described for

Table 1. Explanation of the codes

Code	*Explanation*
AC	Air crystallized
HC	Hydrothermally crystallized
WW	Only water-washed

the AC material. The hydrothermally crystallized ethanol-washed material is coded as HC. In all cases dry-milling was performed with zirconia balls.

The Tosoh TZ-3Y powder was manufactured by the Tosoh Corporation. The Tosoh TZ-3Y powder is a zirconia powder doped with 5·8 at% Y.

2.2 Compaction, sintering and characterization

Green cylindrical compacts were prepared by cold isostatic pressing in two steps: initially at 80 MPa in a rubber tube and finally at 400 MPa in a rubber bag with a 3-min holding time. The green cylindrical compacts had initial dimensions 7–15 mm (height) × 6–7 mm (diameter).

Non-isothermal sintering experiments were performed at temperatures varying from 800 to 1250°C. Isothermal experiments were done at 1050, 1070 and 1150°C for 5–10 h. Heating rates were in all cases 2°C/min; cooling rates 4°C/min. Green and sintered densities were measured by the Archimedes' technique (in Hg).

The relative magnitude of friction between particles in a powder mass is estimated by the ratio of the tap density (TD) to the apparent density (AD) of that mass. This ratio TD/AD is termed the Hausner Ratio[14] and is small for a good flowable powder. The apparent density is the density of a powder after it is poured into a tube without applying any external force. The tap density is the density of the powder after tapping the tube until no volume change is recorded.

Nitrogen adsorption/desorption measurements were performed at 77 K using a Micromeritics ASAP 2400 system. Mesopore size distributions were calculated from the adsorption branch assuming cylindrical pore shape. Specific surface areas were calculated by the BET method; no corrections for microporosity were necessary. The phase composition was analysed by XRD using a Philips PW 1370 diffractometer with Cu K_α radiation. Peaks were corrected for the $K_{\alpha1}/K_{\alpha2}$ doublet and instrumental broadening. Crystallite sizes of the powders were determined by X-ray line broadening assuming Cauchy line profiles. The agglomerate size was measured with a light-scattering technique, where powder was suspended in water through agitation (Microtrac X100), and verified by SEM (Jeol JSM-35CF or Hitachi S800). The shape of the agglomerates was observed by SEM. SEM was also used to investigate the defect structure of green and sintered compacts. Grain sizes in sintered specimens were determined by the lineal intercept technique from SEM (Hitachi S800) micrographs of polished, thermally etched cuts using $D = 1{\cdot}56\ L$, where L is the average lineal intercept.[15] The surfaces of the SEM specimens were coated with Au to prevent charging.

3 Results

3.1 Powder characteristics

The most important powder characteristics are given in Table 2. The primary crystallite size for all as-prepared powders is the same (8 nm). The Tosoh powder contains crystallites which are about four times as large (34 nm[16]). The surface area (S_{BET}) of the Tosoh powder is much lower than that of the as-prepared powders (≈ 20 m^2/g compared to ≈ 100 m^2/g). The phase analysis by X-ray diffraction revealed that the as-prepared powders were tetragonal and contained only traces of monoclinic zirconia. In contrast, the Tosoh powder clearly contained monoclinic and cubic crystallites.[16]

For the production of defect-poor ceramics the agglomerate size, shape and porosity are of importance. The powders used in this study have an agglomerate size ranging from 8 to 42 μm. The agglomerate size of the wet-milled powders is small: 13 μm for the AC and 8 μm for the HC powder. The agglomerate size of the dry-milled AC-WW powder is much larger: 36 μm. The Tosoh powder has an agglomerate size as large as 42 μm.

The agglomerate shape determines to a large extent the packing capability of the powder. A spherical agglomerate causes less friction between the agglomerates than a more irregular agglomerate shape. If the friction is low, it is more likely to have a homogeneous microstructure after compaction. The shape of the dry-milled AC-WW powder is highly irregular as is shown in Fig. 2(a). In Fig. 2(b) the shape of the wet-milled powders is shown. The shape of these agglomerates is somewhat more spherical but still rather irregular. The spray-dried Tosoh powder has a much rounder agglomerate shape, see Fig. 2(c). These agglomerates show a homogeneous morphology.

The mesopore size and pore volume of the powders were measured by nitrogen adsorption.

Table 2. Characteristics of investigated powders

Powder	*Crystallite size (nm)*	*Crystal structure*	S_{BET} (m^2/g)
AC–WW	8	t	100
AC	8	t	100
HC	8	t	99
Tosoh*	34	m: 16%; t: 74% c: 10%	21

m: monoclinic; t: tegragonal; c: cubic.
*Taken from Ref. 16.

The AC and HC powder have approximately the same mean pore diameter (10 nm). In the AC-WW powder the pores are much smaller (6 nm). For the Tosoh powder no mean pore size could be measured because most of the pores are too large to be measured by nitrogen adsorption.

The pore volume of the intra-agglomerate pores was used for calculating the agglomerate porosity. The porosity of the agglomerates gives an indication of the strength of the agglomerates.[17] The agglomerate porosity ϵ_{aggl} is calculated by:[16]

$$\epsilon_{aggl} = \frac{V_p \rho_{th}}{(V_p \rho_{th} + 1)} \quad (1)$$

where ρ_{th} is the theoretical density (6·06 g/cm^3), and V_p is the volume (in units of gram powder) of the nitrogen which is adsorbed in the intra-agglomerate pores as determined by nitrogen adsorption/desorption measurements. The agglomerate porosities obtained in this way are given in Table 3. From these results it is clear that the AC-WW powder contains rather dense agglomerates (porosity 44%). Washing the hydrous-gel with ethanol increases the agglomerate porosity markedly (72 instead of 44%). The use of hydrothermal crystallization instead of crystallization in air reduces the agglomerate porosity somewhat (67 instead of 72%). The agglomerate density of the Tosoh powder is comparable to the agglomerate density of crystallized ethanol-washed gel (air-calcined or hydrothermal crystallized) (64%).

Values for both apparent and tap densities of the powders together with the Hausner Ratios are also given in Table 3. The AC-WW powder has a rather high apparent density. The Hausner Ratio is dependent on the processing method of the powder. The irregular-shaped agglomerates produced by wet-milling result in a Hausner Ratio between 1·6 and 1·8. The round granules produced by spray-drying result in a much smaller Hausner Ratio and thus a better flowability of the powder. The Hausner ratio for the Tosoh powder is as small as 1·1.

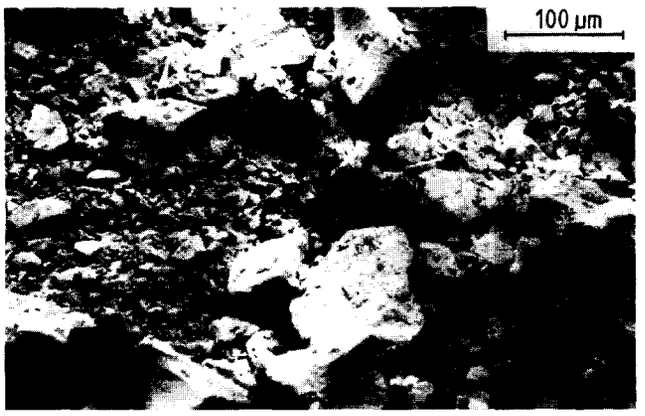

(a)

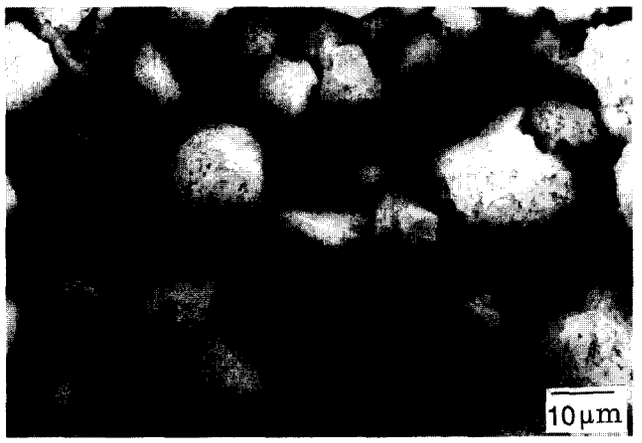

(b)

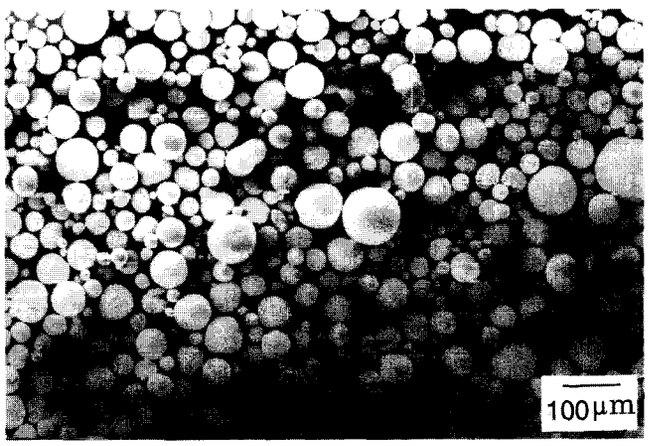

(c)

Fig. 2. (a) Agglomerate shape of powder made by air-calcination of water-washed gel; (b) agglomerate shape of the wet-milled powders (AC and HC); (c) granule shape of Tosoh powder.

3.2 Compaction behaviour

The powders were isostatically pressed up to 400 MPa. After each compaction step, overall density measurements were performed. The relative densities were plotted as a function of the logarithm of the applied pressure (Fig. 3). Most curves show two linear parts with a point of intersection at pressure P_y. The second linear part (at high pressures) can be described by the empirical equation:[16,18,19]

$$\rho - \rho_y = m \times \ln[\frac{P}{P_y}] \quad (2)$$

where m is a constant, ρ the density and P the pressure. The subscript y stands for yield point. The values of P_y and m are given in Table 3.

According to van de Graaf *et al.*[11] the intersection P_y represents the strength of the largest microstructural element. After compaction at a pressure around P_y these elements are all gradually

Table 3. Flow behaviour and agglomerate characteristics of investigated powders

Powder	*AD*	*TD*	*Hausner ratio*	ϵ_{agg} *(%)*	P_y *(MPa)*	m
AC-WW	20·1	27·2	1·4	44	<400 MPa	—
AC	10·1	16·5	1·6	72	72	12
HC	10·2	18·2	1·8	67	60	10
Tosoh*	20·6	22·9	1·1	64	40	7

*Taken from Ref. 16.

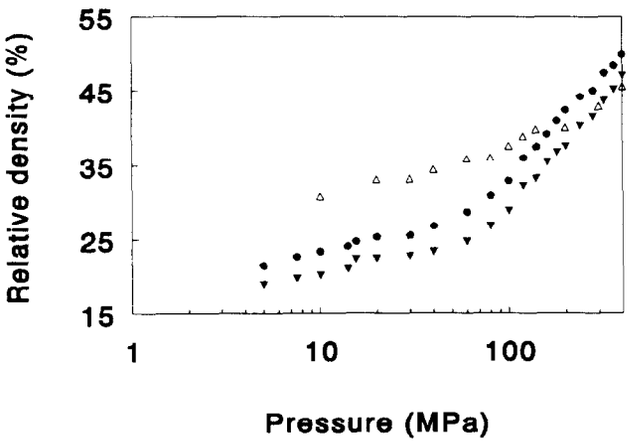

Fig. 3. Compaction behaviour of as-prepared powders. △: AC-WW; ▼: AC; ●: HC.

fragmented, while they are only rearranged at pressures below P_y The largest microstructural elements in this case are the agglomerates.

Powder AC-WW does not show a clear yield point. This implies that the agglomerates are not fractured even at pressures of 400 MPa. For the ethanol-washed gel the agglomerate strength of the air-calcined material is somewhat larger than the agglomerate strength of the hydrothermally crystallized powder (72 MPa compared to 60 MPa). Even though the difference is small the result could be confirmed with another powder batch. The Tosoh powder has a P_y of 40 MPa which is clearly lower than the results obtained with the other materials (60–75 MPa).

The value of m is related to the behaviour of the powder during compaction. A large value of m corresponds to a relatively rapid increase in relative density with compaction pressure. A large value of m may be an indication for a large overall density variation in the green compact. During compaction the stress distribution in a compact is not uniform throughout the powder compact due to the frictional forces between powder particles. With high values of m, small stress deviations will lead to large density variations. Large overall density distributions in a specimen may result in fracture during unloading or ejecting of the specimen, especially when large specimens are made. The m values of the various powders range between 7 and 12. It is expected that the density distribution created during compaction of the Tosoh material is small, therefore, it should be easy to prepare large samples of this material.

3.3 Green compact structure

Mesopores were measured by nitrogen adsorption. The pore size distributions in compacts after isostatic pressing at 400 MPa of AC-WW and AC are given in Fig. 4. The pore size distribution of the HC material is similar to that of the AC material. The most frequently found pore diameter as measured from desorption for Tosoh compacts is 50–60 nm.[16] Note that this pore diameter has been measured from the desorption branch and so underestimates the real diameter. The most frequently found pore diameter of the AC and HC compacts is the same and equals 9·5 nm; the mean pore diameter is 6·6 nm. The AC-WW material has somewhat smaller pores (8 nm) and a smaller distribution; the mean pore diameter is 6·0 nm.

Large pores (second generation) were analysed by SEM. Figure 5(a) shows the fracture surface of a AC-WW green compact. Here the agglomerate structure can easily be identified as shown by the arrow. Figure 5(b) shows the structure of an AC and HC green compact. Although the agglomerates are fractured during compaction, the agglomerate form still persists inside the green compact. In some cases, interagglomerate pores can be seen. Those pores are very large (1–2 μm) in comparison to the crystallite size (8 nm).

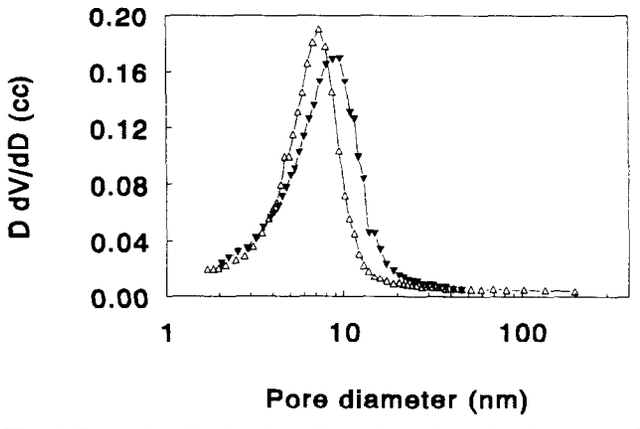

Fig. 4. Pore size distribution (from the adsorption branch) of green compacts made from air-calcined water-washed (△; AC-WW) and ethanol-washed (▼; AC) gel.

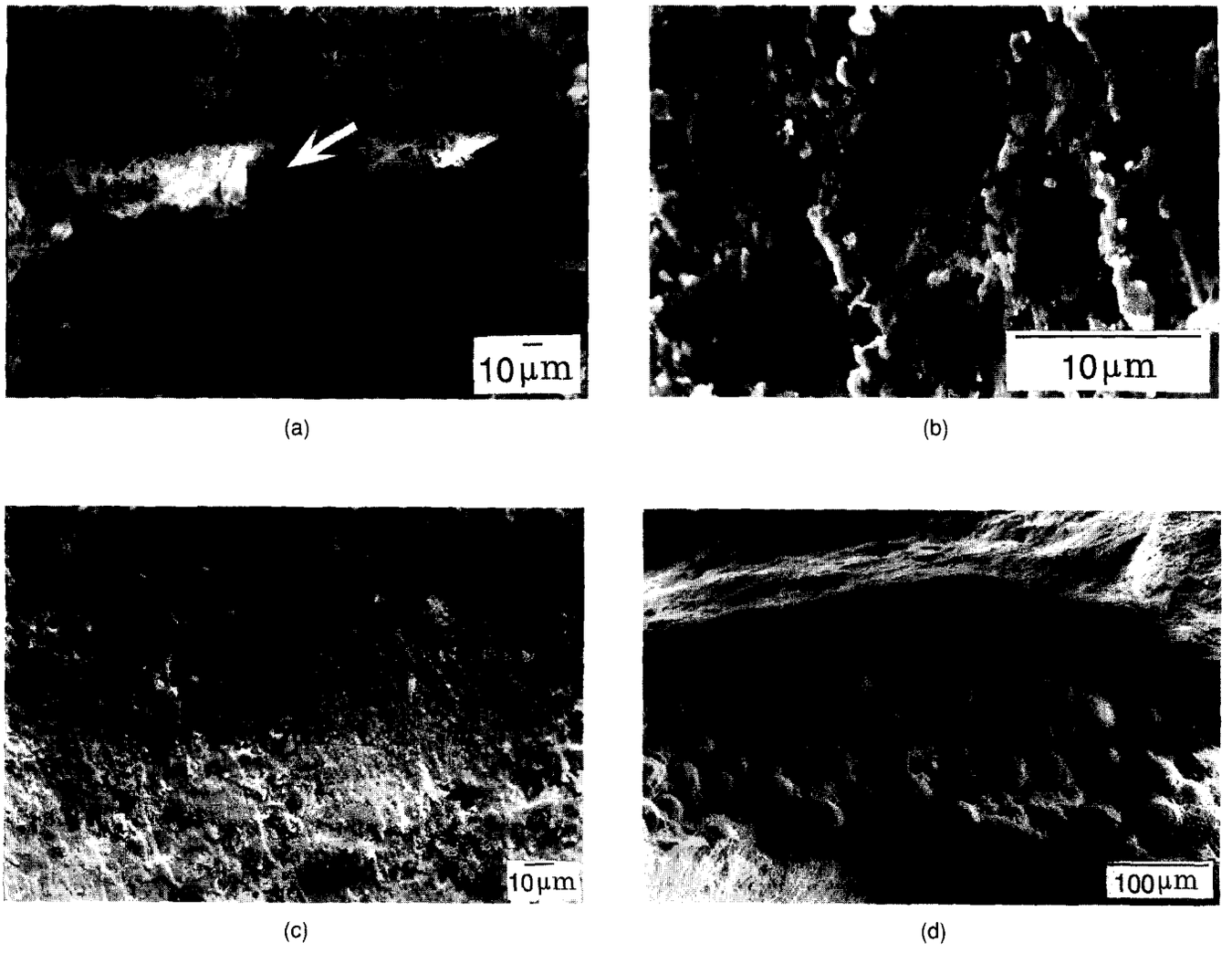

Fig. 5. Fracture surface of green compact prepared from (a) air-calcined water-washed gel (AC-WW); (b) air-calcined (AC) or hydrothermally crystallized (HC) ethanol-washed gel; (c) inhomogeneity in green compact prepared from air-calcined (AC) or hydrothermally crystallized (HC) ethanol-washed gel; (d) fracture surface of green compact Tosoh with clear 'residual' granule structure.

Fig. 5(c) shows an inhomogeneity in the green compact found for both AC and HC compacts. This inhomogeneity might originate from a very strong agglomerate which does not fracture completely upon pressing.

The green compact structure of the Tosoh material is very homogeneous. The granule shape of the powder is also in this case easily recognized on a fractured surface (Fig. 5(d)).

3.4 Microstructural evolution during sintering

The maximum attainable density for the materials analysed in this work varied markedly. The as-prepared materials all contain some porosity after sintering for 10 h at 1150°C. The porosity of the HC material equals 2%, that of the AC material is 8%. The porosity of the AC-WW material is extremely high: 20%. The sintered density of the as-prepared materials could not be increased by using other sintering schedules. The as-prepared materials have an ultra-fine grain size of 0·18 μm after sintering for 10 h at 1150°C. To obtain an even smaller grain size, isothermal sintering experiments were performed with the hydrothermally crystallized material at 1050 and 1070°C with a dwell time of 5 and 10 h, respectively. In both cases this resulted in a decrease of sintered density (93 and 95%, respectively) and a decrease of the grain size to 95 and 120 nm, respectively. Thus, the hydrothermally crystallized materials are very interesting for the production of nanostructured ceramics but cannot be produced defect-free at this moment.

The Tosoh material has a relatively low sinter activity and must be sintered at a higher temperature to achieve a high density. After sintering at 1400°C without isothermal hold the Tosoh material achieved a density of 99%. Unfortunately, the Tosoh material cannot be prepared ultra-fine-grained due to this high sinter temperature. After sintering at 1400°C without isothermal dwell the Tosoh material has a grain size of 0·3 μm.[18] Ultra-fine grains result after sintering at 1200°C without isothermal dwell (0·15 μm) but then the density of

this material is only 76%.[18] Thus, the Tosoh material can be made defect-poor but not nanostructured.

Pores in the sintered material can be attributed to first- or second-generation pores. Intra-aggregate pores could not be found in the sintered material. In the following the evolution of first- and second-generation pores during sintering will be described in detail.

3.4.1 Evolution of first-generation pores

The pore structures of as-prepared powder compacts are quite similar up to 1000°C. Therefore, the porosity change of only one material (AC) is shown. Figure 6 shows the pore size distributions for a green compact and after non-isothermal sintering at 800, 900 and 1000°C. During heating to 1000°C the density increased by approximately 15%. It is clear that while the porosity decreases the pore size increases. The most frequently found pore diameter increases from 9·5 nm to 33 nm. For the AC-WW compact the most frequently found pore diameter increases from 8 nm to 30 nm. The coarsening of the pores upon heating is in accordance with the results of Boutz *et al.*[19] and Theunissen *et al.*[18] Theunissen *et al.*[18] also found coarsening upon heating for the Tosoh material.

From the evolution of first-generation pores during sintering it cannot be explained why the different as-prepared materials sinter to a different final density.

3.4.2 Evolution of second-generation pores

In the intermediate stage of sintering, stresses induced by differential sintering in powder compacts are most pronounced.[20] All samples were sintered at temperatures between 1000 and 1250°C without isothermal hold (heating rate 2°C /min; cooling rate 4°C/min). The sintering schedule and the densities of the analysed specimens are shown in Table 4. From this table it is clear that

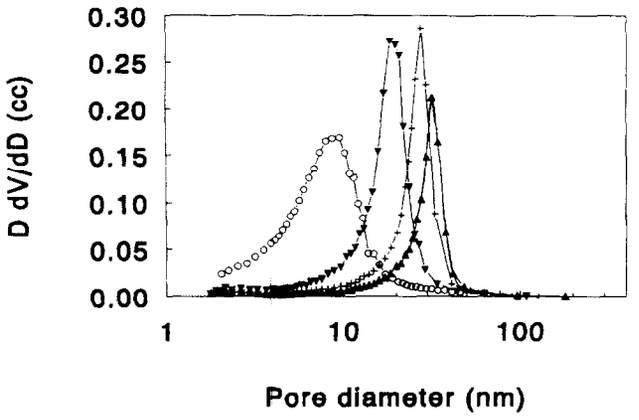

Fig. 6. Pore size distributions of air-calcined ethanol-washed gel (AC) in the green compact (○) before and after heating to (▼) 800, (+) 900 and (▲) 1000°C, as calculated from the adsorption branch of N_2 sorption measurements.

Table 4. Densities of the sintered specimens. Specimens were sintered to the indicated temperature, immediately followed by cooling (heating rate 2°C/min; cooling rate 4°C/min)

T(°C)	*AC-WW* (%)	*AC* (%)	*HC* (%)	*Tosoh* (%)
1000	51	60	62	
1050	59	72	75	
1070	64	77	80	
1200				65
1250				75

although the primary crystallite size of the as-prepared materials is the same, the sintered density at each temperature for the AC-WW material is lower than for the other two as-prepared samples. The AC and HC materials have approximately the same density after non-isothermal sintering at intermediate temperatures. The Tosoh material densifies at a much higher temperature than the ultra-fine materials. This is because of the larger crystallite sizes of the Tosoh material.

The structural evolution of the four materials will be described below in terms of an increasing number of defects in the sintered material. SEM observations on sintered Tosoh compacts show that there are no large pores in the ceramic microstructure at any stage. Still, the material is not totally homogeneous during densification. Figure 7 shows that remainders of agglomerates have been broken out of the surface at a density of 75%. The SEM specimen shown in Fig. 7 was prepared by severe polishing of the ceramic. The observed agglomerate-like structure does not, however, reduce the final sintered density with the result that the Tosoh material can be prepared almost defect-free ($\rho \geq 99\%$).

A final density of 98% is attained at 1150°C for the HC material. This means that a small amount of porosity cannot be removed from the structure. SEM observations have shown that the porosity

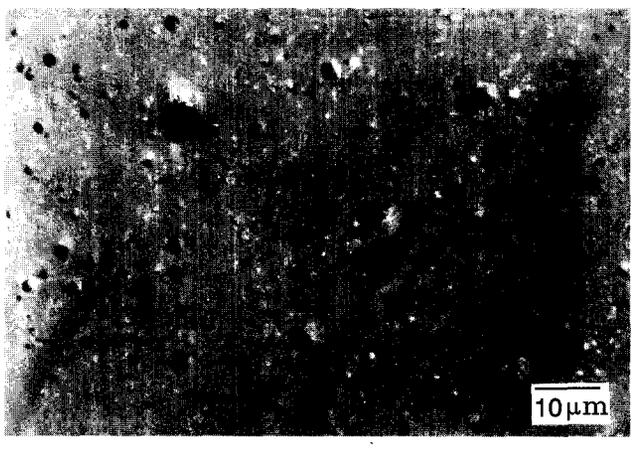

Fig. 7. Surface of Tosoh compact density 75%. The parts pulled out have the same size and shape as the granules.

in these sintered ceramics is solely attributed to defects. Those defects have an elongated or spherical shape and a maximum size of about 30 μm (Fig. 8). The defects found in the fully densified material have the same size and shape as the defects found in a sintered compact with a density of 60%. Because these large defects (30 μm) are not found in the green compacts, they must be formed during sintering.

A maximum final density of 92% can be achieved with the AC material. In the sintered material both singular defects and defect clusters can be found (see Fig. 9). The singular defects have the same shape and size as the defects found in the HC material. The occurrence of defect clusters in the sintered ceramic is the reason why the final density is so limited in case of the AC material. The inhomogeneities found in an AC sample sintered to 60% (Fig. 10) density is probably the origin of the defect clusters in the fully densified material. The porosity inside the inhomogeneity seems to be different from the porosity inside the remainder of the compact. Based on the size and the internal structure of the inhomogeneity it is concluded that the inhomogeneity is basically a single agglomerate with a different internal structure than the other agglomerates.

A final density of only 80% can be achieved with the AC-WW material. In the sintered material, an agglomerate-like structure can be recognized (Fig. 11). The structure within the agglomerates is completely dense.

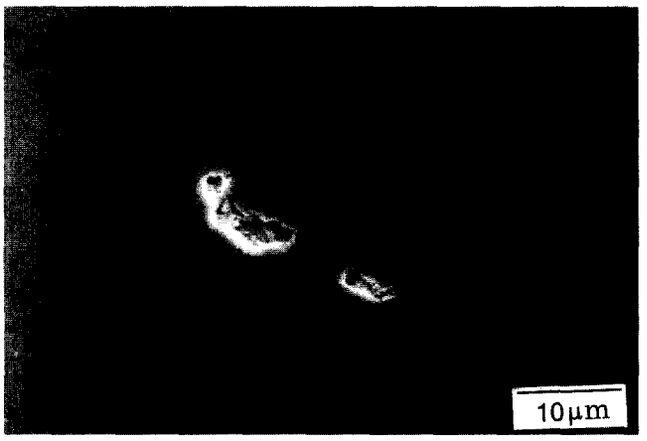

Fig. 8. Defect found in 98% dense hydrothermally crystallized (HC) material.

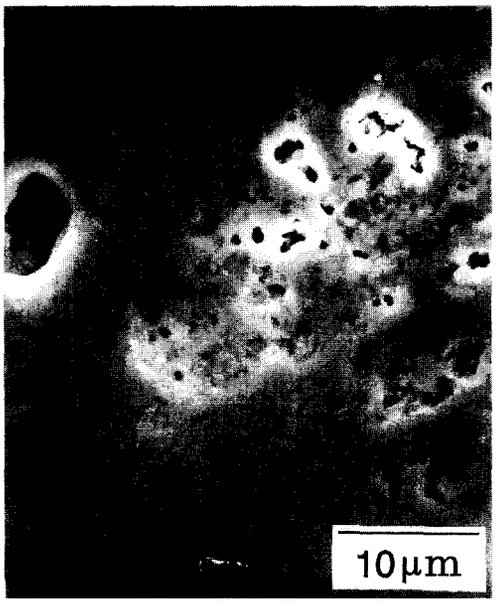

Fig. 9. Defect and defect cluster in dense (92%) material prepared from air-calcination of ethanol-washed gel particles (AC).

4 Discussion

4.1 Origin of defects

In a green compact a mixture of small (first-generation) and large (second-generation) pores is usually found. The large pores are always more difficult to remove for two basic reasons. First, simple kinetics dictates a longer time to fill a larger void by diffusion.[21] Second, as pointed out by Kingery and Francois,[22] a large pore can be thermodynamically stable depending on the value

Fig. 10. Inhomogeneity in 60% dense material prepared from air-calcination of ethanol-washed gel particles (AC).

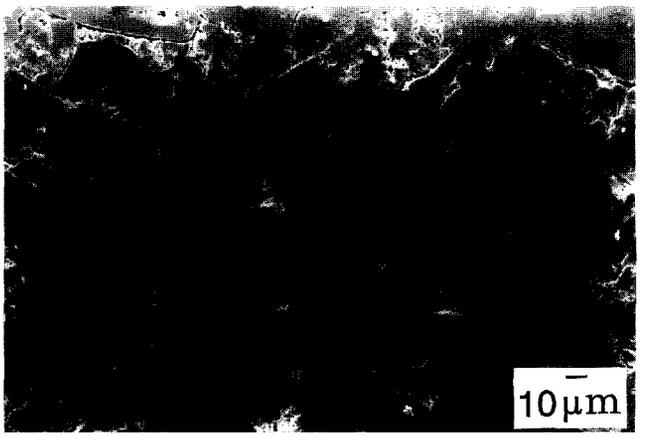

Fig. 11. 'Residual' agglomerate structure visible in 80% dense material prepared from air-calcination of water-washed gel particles (AC-WW).

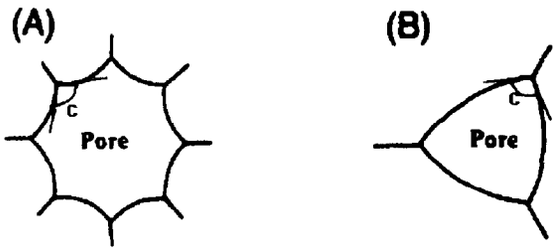

Fig. 12. (a) Thermodynamically stable pore configuration. Grain size smaller than critical. (b) Thermodynamically unstable pore configuration. Grain size larger than critical. Dihedral angles (c) are equal.

of the dihedral angle and the pore size/grain size ratio. Figure 12 illustrates the morphologies of two pores with the same volume, but different coordination numbers. The dihedral angle is the same for both pores. Looking from within, the pore with the higher coordination number (A) has convex surfaces, whereas the surfaces of the pore with the lower coordination number (B) are concave. In general, for a given dihedral angle, a critical coordination number, D_{critical}, exists that defines the transition from convex ($D > D_{\text{critical}}$) to concave ($D < D_{\text{critical}}$) surfaces. Kingery and Francois were the first to recognize that only those pores with $D < D_{\text{critical}}$ are able to disappear during sintering.

In the as-prepared green compacts both small and large pores can be found. The small pores disappear upon sintering whereas the large pores grow. The pore size of the large pores remains much larger than the critical pore size. Therefore, the maximum density that can be achieved is limited by the volume fraction of large pores present initially.

Most inter-agglomerate porosity is removed from the AC, HC and Tosoh materials during compaction. This suggests that the agglomerate strength of those powders is low enough. The AC-WW material has a very high agglomerate strength. The defects in the AC-WW material are related to the dense, strong agglomerates present in the powder.

The defects in the green compacts of the wet-milled ZY5 materials (AC and HC) are a result of the irregular agglomerate shape and the resulting poor flowability of the powder. These irregular agglomerates result in inhomogeneous filling of the die resulting in stacking flaws.

The small defects (1–2 μm), found in the green compacts of AC and HC materials, grow during sintering to sizes < 30 μm. The growth of the defects can be explained by the model of Veringa.[23,24] In this model it is recognized that a stacking of spherical particles having local variations in their individual coordination will exert a pressure on its immediate surroundings.[24] This pressure is determined by both the total and local coordination. If somewhere in the stacking of particles a gradient exists in the local coordination, it is concluded that a force is acting on the particle considered into the direction of the area with highest coordination. The force generates a pressure which stimulates densification in zones with a relatively high stacking density (high density) and causes dilution at places where the stacking density is lower than average (low density). This pressure will finally result in the formation or growth of flaws (defects) in the ceramic. The experimental results are in qualitative agreement with these models.

The defects grow to their final size at intermediate temperatures and do not grow further at higher temperatures. This can be explained by the development of maximum stress at intermediate temperatures.[20]

4.2 Defect clusters

Defect clusters are only found in the AC material. The green compact structures of the AC and HC compacts appear to be similar; both materials contain inhomogeneities. Because defect clusters can be found in the sintered AC material but not in the sintered HC material it is concluded that the defect clusters found in the AC material are formed during sintering. These defect clusters are probably a result of different individual agglomerate structures inside the powder which must originate from the powder synthesis. The only difference between the AC and the HC powder synthesis is the crystallization medium, respectively air and water. Before crystallization both powders are first washed with water, then ethanol and subsequently dried. If ethanol washing is not performed thoroughly enough, the gel will not be dispersed well and lumps of water-washed gel will persist in the ethanol-washed gel (see Fig. 13). After drying, the former water-rich parts will be more dense than the former ethanol-rich parts due to the larger capillary forces during drying in the water-rich area resulting in both strong and weak agglomerates. For hydrothermal crystallization

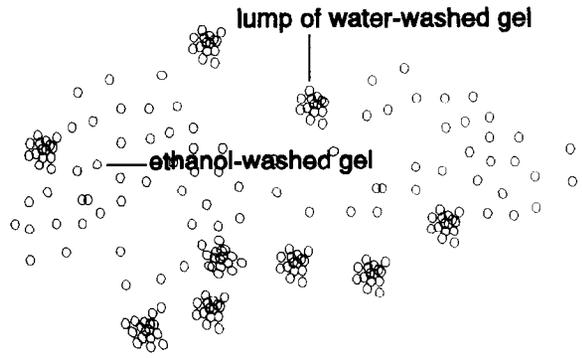

Fig. 13. Schematic of ethanol-washed gel structure.

the ethanol-washed and dried gel is added to a dilute ammonia solution. It can be argued that during hydrothermal treatment all ethoxy groups adsorbed on the surface of the gel are replaced by hydroxy groups giving rise to equal strength of the bonds inside the crystallized agglomerates. After hydrothermal crystallization a more homogeneous structure is obtained.

Based on these arguments it is concluded that in the AC powder two types of agglomerates are present differing in density and pore size. The pore structure in a powder compact made from different kinds of agglomerates will be inhomogeneous. Veringa[23,24] has, among others, shown that an inhomogeneous packing density will lead to differential sintering. The strong agglomerates lead to defect clusters, whereas the weak agglomerates do not.

In the current work it is hypothesized that a zirconia matrix made up of weak agglomerates exists in the AC material which contains, however, a number of strong agglomerates. Those strong agglomerates are not fractured during consolidation. This means that a variation in pore sizes present in the powder for statistical reasons can still be found in the green compact. The best way to prevent the formation of strong agglomerates in the air-crystallized ethanol-washed powder is probably by improving the ethanol-washing step during powder synthesis by an improved mixing procedure.

5 Conclusions

- Ultra-fine ceramics of yttria-doped tetragonal zirconia (grain size 0·12–0·18 μm) can be prepared with limited porosity (4%–2%) in a low temperature (1070–1150°C) sintering process. The residual porosity is attributed to defects.
- Defect-poor ceramics can be prepared if the powder consists of homogeneous dense, spherical agglomerates (density $\geq$ 99%). However, those ceramics are not ultra-fine (grain size 0·3 μm) due to the relative high sinter temperature used.
- Defects found in the sintered materials are already present in the green compact.
- Small defects in the green compact increase in size during the earlier stages of sintering.
- The agglomerates of the powder prepared by crystallization in air of a gel water-washed only are too strong to result in a homogeneous green compact during compaction.
- The defect clusters in the air-calcined material made from an ethanol-washed gel are probably caused by strong agglomerates.
- The irregular agglomerate shape of the wet-milled air-calcined and hydrothermally crystallized powders made from an ethanol-washed gel results in improper die filling, resulting in defects in the green compact.

Acknowledgements

These investigations were partly supported by the Innovative Research Program on Technical Ceramics (IOP-TK) with financial aid from the Dutch Ministry of Economic Affairs.

References

1. He, Y. J., Winnubst, A. J. A., Burggraaf, A. J. & Verweij, H., Grain size dependence of sliding wear in tetragonal zirconia polycrystals. *J. Am. Ceram. Soc.*, in press.
2. He, Y. J., Tribological and mechanical properties of fine-grained zirconia and zirconia–alumina ceramics. PhD thesis, University of Twente, Enschede, The Netherlands, 1995.
3. Theunissen, G. S. A. M., Bouma, J. S., Winnubst, A. J. A. & Burggraaf, A. J., Mechanical properties of ultra-fine-grained zirconia ceramics, *J. Mater. Sci.*, **27** (1992) 4429–4438.
4. Theunissen, G. S. A. M., Microstructure, fracture toughness and strength of (ultra)fine-grained tetragonal zirconia ceramics. PhD thesis, University of Twente, Enschede, The Netherlands, 1991.
5. Boutz, M. M. R., Winnubst, A. J. A., Burggraaf, A. J., Nauer, M. & Carry, C., Low temperature sinter forging of nanostructured Y-TZP and YCe-TZP. *J. Am. Ceram. Soc.*, **78**(1) (1995) 121–128.
6. Winnubst, A. J. A., Boutz M. M. R., He, Y. J., Burggraaf, A. J. & Verweij, H., (Super)plasticity of nanocrystalline zirconia ceramics. In *Ceramics: Charting the Future*, ed. P. Vincenzini. Techna Srl, Faenza, Italy, 1995, pp. 1743–1754.
7. Niesz, D. E., Bennett, R. B. & Snyder, M. J., Strength characterization of powder aggregates. *Am. Ceram. Bull.*, **51**(9) (1972) 667–680.
8. Halloran, J. W., Role of powder agglomerates in ceramic processing. In *Advances in Ceramics*, Vol. 9., ed. J. A. Mangels & G. L. Messing. The American Ceramic Society, Inc., Columbus, Ohio, 1984, pp. 67–75.
9. Halloran, J. W., Agglomerates and agglomeration in ceramic processing. In *Ultrastructure Processing of Ceramics, Glasses and Composites*, ed. L. L. Hench & D. R. Ulrich. John Wiley & Sons, New York, 1984, pp. 404–417.
10. Lecloux, A. J., Verleye, P., Bronckart, J., Novillc, F., Marchot, P. & Pirard, J. P., Texture and sintering of zirconium dioxide–yttrium oxide ceramics. *Reactivity of Solids*, **4** (1988) 309–325.
11. Van de Graaf, M. A. C. G., ter Maat, J. H. H. & Burggraaf, A. J., Microstructure and sintering kinetics of highly reactive ZrO_2–Y_2O_3 ceramics. *J. Mater. Sci.*, **20** (1985) 1407–1418.
12. Lange, F. F. & Metcalf, M., Processing-related fracture origins: II, Agglomerate motion and cracklike internal surfaces caused by differential sintering. *J. Am. Ceram. Soc.*, **66**(6) (1983) 398–406.
13. Lange, F. F., Processing-related fracture origins: I, Observations in sintered and isostatically hot-pressed

Al_2O_3/ZrO_2 composites. *J. Am. Ceram. Soc.*, **66** [6] (1983) 396–398.
14. Hausner, H. H., Friction conditions in a mass of metal powder. *Intern. J. Powder Metal.*, **3**(4) (1967) 7–13.
15. Mendelson, M. I., Average grain size in polycrystalline ceramics. *J. Am. Ceram. Soc.*, **52** (1969) 443–446.
16. Groot Zevert, W. F. M., Winnubst, A. J. A., Theunissen, G. S. A. M. & Burggraaf, A. J., Powder preparation and compaction behaviour of fine-grained Y-TZP, *J. Mater. Sci.*, **25** (1990) 3449–3455.
17. Rumf, H., Grundlagen und Methoden des Granulierens. *Chemie-Ing.-Techn.*, **30** (1958) 144–158.
18. Theunissen, G. S. A. M., Winnubst, A. J. A. & Burggraaf, A. J., Sintering kinetics and microstructure development of nanoscale Y-TZP ceramics. *J. Eur. Cer. Soc.*, **11** (1993) 315–324.
19. Boutz, M. M. R., Winnubst, A. J. A. & Burggraaf, A. J., Yttria-ceria stabilized tetragonal zirconia polycrystals: sintering, grain growth and grain boundary segregation. *J. Eur. Ceram. Soc.*, **13** (1994) 89–102.
20. Kellett, B. & Lange, F. F., Stresses induced by differential sintering in powder compacts. *J. Am. Ceram. Soc.*, **6**(5) (1984) 369–371.
21. Herring, C., Effect of change of scale on sintering phenomena, *J. Appl. Phys.*, **21** (1950) 301.
22. Kingery, W. D. & Francois, B., Sintering of crystalline oxides, I. Interactions between grain boundaries and pores. In *Sintering and Related Phenomena*, ed. G. C. Kuczynski, N. A. Hooton & G. F. Gibbon. Gordon & Breach, New York, 1967, pp. 471–498.
23. Veringa, H. J., Statistical treatment of the sintering defect model and ceramic morphology development. *J. Mater. Sci.*, **28** (1993) 2757–2762.
24. Veringa, H. J., An alternative way of looking at sintering models and the development of instabilities. *J. Mater. Sci.*, **26** (1991) 5985–5995.